International Journal of Offshore and Polar Engineering
Vol. 14, No. 4, December 2004 (ISSN 1053-5381)

A Microstructural Study of Friction Stir Welded Joints of Carbon Steels

A. Ozekcin, H. W. Jin, J. Y. Koo*, N. V. Bangaru and R. Ayer*
ExxonMobil Research and Engineering Company, Annandale, New Jersey, USA

G. Vaughn
Formerly with ExxonMobil Upstream Research Company, Houston, Texas, USA

R. Steel and S. Packer
Megastir Technologies, Provo, Utah, USA

ABSTRACT

Friction Stir Welding (FSW) is an emerging technology that has made significant inroads in the joining of aluminum alloys in the aerospace industry. To explore the potential advantages in joining carbon steels by FSW, the present study focuses on microstructure characterization of friction stir welded API grade X80 and L80 steels using SEM, TEM and SIMS. The study focuses on the mechanisms of microstructure evolution at various regions of the FSW joint, resulting from the effect of strain, temperature and tool interaction on the phase transformations. A qualitative comparison of the microstructural features between friction stir welds and typical fusion welds in these steels is also presented.

INTRODUCTION

Friction stir welding (FSW) is a solid state materials joining process invented by TWI (Thomas et al., 1991) that has been widely investigated by various researchers in mostly low melting, aluminum alloys. The application of FSW to the joining of steels and other high- temperature materials has been limited primarily by the absence of suitable tool material that can operate at high temperatures in the 1000∼1200°C range (Threadgill and Johnson, 2004; Packer et al., 2003). Even though considerable improvements in high-temperature tool materials have been made recently, only a limited amount of work has been reported on the FSW of steels (Johnson et al., 2003; Konkol, 2003; Lienert et al., 2003; Lienert, Tang and Kvidahl, 2003; Okamoto et al., 2003; Posada et al., 2003).

X80 and L80 API-grade steels are typically used in several oil and gas operations. Although these steels have comparable strength, they have significantly different chemistry, and they are produced by fundamentally different metallurgical processes. X80 is produced by thermomechanically controlled processing (TMCP) while L80 is produced by the quench and temper (Q/T) process. The microstructure and mechanical properties of FSW joints depend on the chemistry and processing history of base material as well as FSW parameters. Also, as discussed elsewhere, the effects of the FSW process on the microstructure of steel joints are expected to be significantly different from those of the aluminum alloy joints (Threadgill and Leonard, 1999). The objective of the present work, then, was to investigate the microstructural evolution in FS-welded X80 and L80 steels using the state-of-the-art characterization methods.

*ISOPE Member.
Received August 28, 2004; revised manuscript received by the editors November 2, 2004. The original version (prior to the final revised manuscript) was presented at the 14th International Offshore and Polar Engineering Conference (ISOPE-2004), Toulon, France, May 23–28, 2004.
KEY WORDS: Friction stir welding, FSW, carbon steels, X80, L80, microstructure, microhardness.

EXPERIMENTAL PROCEDURE

X80 and L80 with different thickness, 20 mm and 8 mm, respectively, were used in the FSW studies. The chemical compositions of the steels (wt.%) are:

X80–0.13 C, 1.52 Mn, 0.26 Si, 0.17 Mo, 0.034 Cr, 0.026 Ni, 0.0002 Nb, 0.003 Ti, 0.062 V, 0.041 Al, 0.032 Cu, 0.0003 B.

L80–0.32 C, 1.20 Mn, 0.35 Si, 0.65 Mo, 1.30 Cr, 0.20 Ni, 0.04 Nb, 0.04 Ti, 0.05 V, 0.04 Al, 0.20 Cu, and 0.0025 B

The carbon equivalent values, Ceq, of X80 and L80 steels were calculated to be 0.44 and 0.94, respectively (Honeycombe and Bhadeshia, 1995).

Test plates were sectioned in half along the rolling direction and prepared for a butt joint. Oxide scale was removed by sand grinding followed by degreasing with methanol. During FSW, loads along the X-, Y- and Z-axis were recorded along with the tool temperature from a thermocouple placed in the tool shoulder. An argon gas atmosphere was used to prevent oxidation during the weld cycle and to prolong tool life.

Table 1 gives the FSW parameters for both steels. A polycrystalline cubic boron nitride (PCBN) tool was used in this study. The PCBN tool configuration and shoulder design are described elsewhere (Packer et al., 2003). FSW was performed in a single-sided, partial penetration mode.

The X80 steel was welded using a single set of parameters, while the L80 steel was welded with 2 sets. The 2 welding conditions for the L80 steel will be referred to as L80-1 and L80-2.

		FSW Parameters		
ID	Material	Tool rotation	Z-load	Travel speed
X80	X80 Steel	550 rpm	5500 lb	4 ipm
L80-1	L80 Steel	450 rpm	9000 lb	4 ipm
L80-2		550 rpm	7000 lb	4 ipm

ipm: inch per min; rpm: rotation per min

Table 1 FSW processing parameters

In addition, typical fusion welds (FW) by submerged arc welding (SAW) of these steels were also examined for comparison.

Metallographic samples for optical, SEM, TEM, SIMS and microhardness investigations were prepared from weldments using standard metallographic procedures followed by etching with 2% nital solution. Secondary ion mass spectroscopy (SIMS) was performed using a Cameca IMS 3F SIMS system. Scanning electron microscopy (SEM) was performed in a JEOL 840A microscope; transmission electron microscopy study was performed in a Philips CM200 FEG microscope. Vickers microhardness traverses were recorded using a 100-gram load and 15-s dwell time. Thin foils for TEM studies were prepared by cutting from specimens from selected areas of the weldments, mechanically thinned down, and electrochemically polished using a twin jet polisher with a 30-ml perchloric acid, 175-ml butanol, and 300-ml ethanol solution at −40°C.

RESULTS

Fig. 1 shows low magnification optical images of weld cross-sections indicating various regions of the FSW of X80 and L80-1 and L80-2 samples.

It has been recognized that it is difficult to delineate the HAZ/TMAZ boundaries in steels as a result of the phase transformations (Threadgill and Leonard, 1999). Thus the locations of these boundaries indicated in this paper are only approximate, based on the contrast observed in the macro images.

Microhardness

Fig. 2 shows microhardness profiles from FSW samples of X80 and L80 steels. The weldment of the X80 steel shows several features: very little HAZ softening; overall higher hardness of the weld compared to the base metal; and a hard zone within the TMAZ at the advancing side of the weld. In both L80-1 and L80-2, HAZ hardening was observed, and TMAZ hardness was significantly higher than that of HAZ and base metal. In L80-1, average TMAZ hardness was 360 DPH, increasing to the 500-DPH level at the hard zone toward the advancing side of FSW. In L80-2, overall TMAZ hardness was about 420 DPH. In this sample, the presence of a hard zone was not apparent in the microhardness profile, presumably due to the high TMAZ hardness overall compared with the other samples.

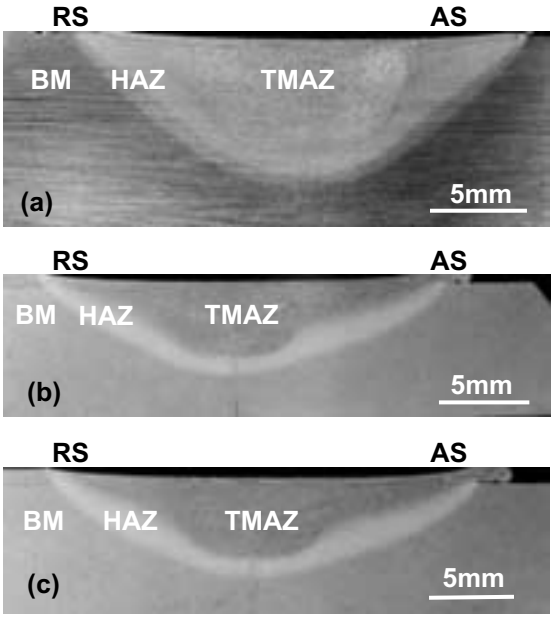

Fig. 1 Optical micrographs of FSW joints: (a) X80, (b) L80-1 and (c) L80-2 (BM = base metal, HAZ = heat-affected zone, TMAX = thermomechanically affected zone, RS = retreating side, and AS = advancing side

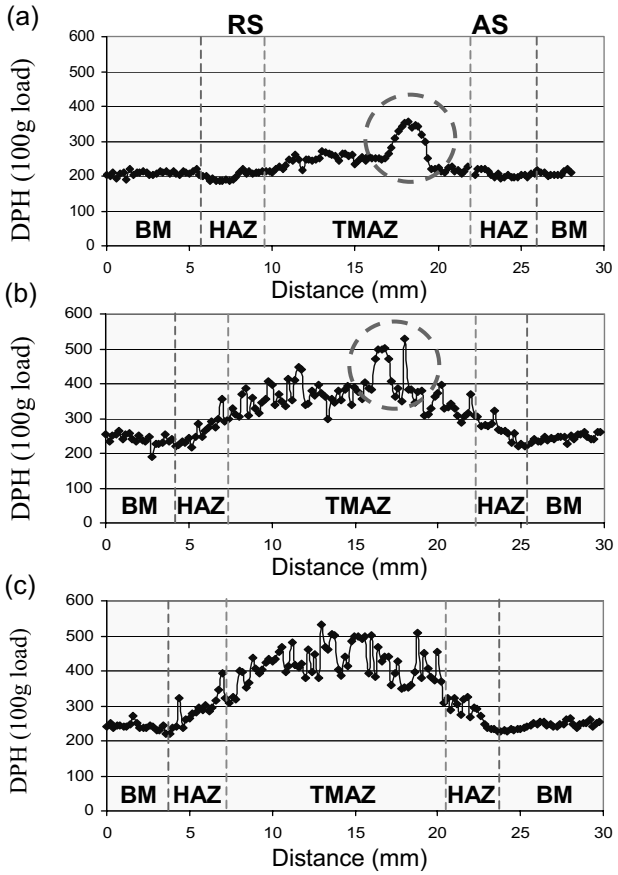

Fig. 2 Microhardness profiles: (a) X80, (b) L80-1, and (c) L80-2; circle = TMAX hard zone (TMAZ-HZ); profiles taken 2.5 mm from center top line

Microstructure Characterization

Base metal. Fig. 3 shows base metal microstructures of X80 steel. The steel base metal is composed of ferrite, granular bainite (GB) and martensite. The details of these microstructural constituents are described elsewhere (Bangaru et al., 2004). The average grain size was 7 μm, and fine ($\leq$100 nm) globular (Nb,Ti)(C,N) precipitates were observed as shown in Fig. 3b.

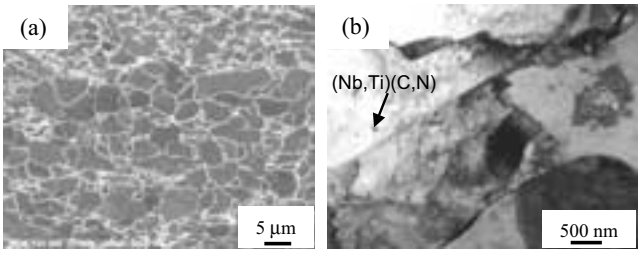

Fig. 3 X80 steel; base metal (BM) microstructure: (a) SEM and (b) TEM images; arrow = (Nb,Ti)(C,N) precipitate

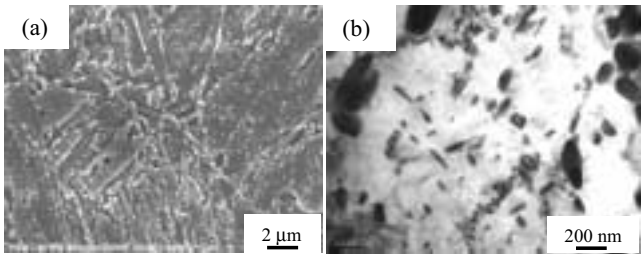

Fig. 4 L80 steel; BM microstructure: (a) SEM and (b) TEM images revealing high density of precipitation of rod-shaped M_2C carbides and globular M_3C carbides

Fig. 4 shows the base metal microstructure of L80 steel. The average grain size was 20 μm with a high density of tempered carbides both inside the ferrite grain and at the grain boundaries. TEM investigation revealed that rod-shaped fine ($\sim$100 nm) precipitates were M_2C-type Mo rich carbides, and coarser ($\sim$300 nm) globular precipitates were M_3C-type carbides.

HAZ Figs. 5 and 6 show the HAZ grain size and microstructures of X80 and L80 steels, respectively. The HAZ grain sizes of all samples were refined compared to that of the base metals.

The HAZ of X80 steel comprises ferrite, GB and lath martensite (LM) with a refined grain size of about 5 μm. Another microstructural feature observed was a reverted austenite particle that indicates the exposure to intercritical temperature. The HAZ of the L80-1 and L80-2 samples exhibited an average grain size of 13 μm and 16 μm, respectively. The coarsening of carbides and evolution of hard martensite microstructure were noted in both samples.

TMAZ Fig. 7 shows SEM and TEM micrographs from the TMAZ region of all 3 samples. In X80, microstructure consisted predominantly of GB, degenerate upper bainite (DUB) and LM. The average grain size in TMAZ was 15 μm, which was much coarser than that in the BM and HAZ. The TMAZ regions of L80 steels exhibited microstructures consisting of lower bainite (LB), DUB, LM and tempered martensite (TmM).

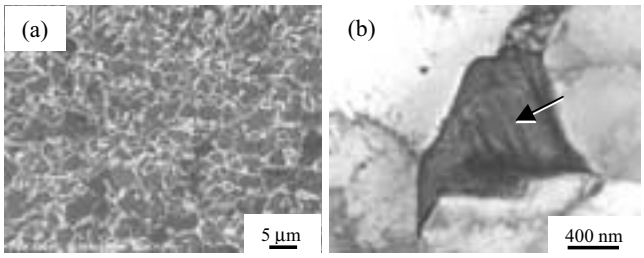

Fig. 5 X80 steel; HAZ microstructure: (a) SEM, and (b) TEM showing reverted austenite and stacking faults (arrow)

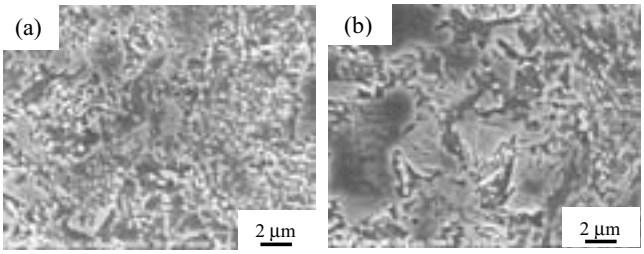

Fig. 6 SEM HAZ microstructure: (a) L80-1 and (b) L80-2

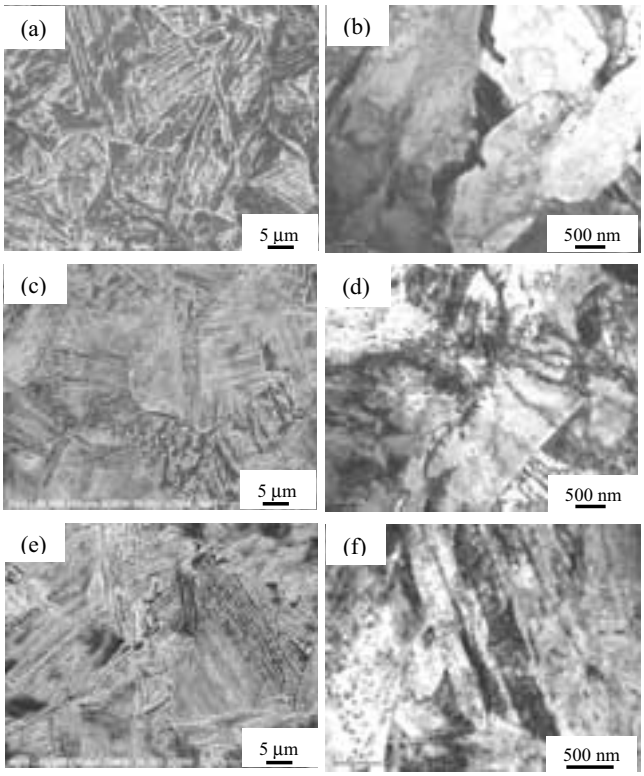

Fig. 7 TMAZ microstructures: (a) and (b) = X80; (c) and (d) = L80-1; (e) and (f) = L80-2

The L80-2 sample exhibited a higher volume fraction of acicular structures such as LM than the L80-1 sample, which showed more LB and TmM as the dominant microstructure. Also noted was that these regions had coarse grain size, e.g. 25 μm in L80-1, 30 μm in L80-2.

TMAZ-HZ The TMAZ-HZ is the hardest region in the weldments of the 3 samples (Fig. 2). It also exhibits coarser grain size than the HAZ and TMAZ in X80 and L80-1, and comparable grain size in L80-2 (Table 2). In addition, a banded structure was

	Average Grain Size (μm)			
Sample ID	BM	HAZ	TMAZ	TMAZ HZ
X80	7	5	15	30
L80 -1	20	13	25	30
L80 -2	20	16	30	28

ipm: inch per min; rpm: rotation per min

Table 2 Grain sizes of X80, L80 welds

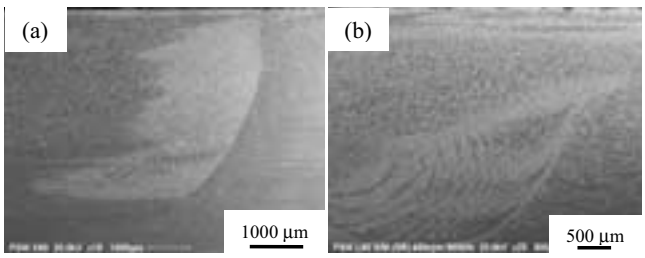

Fig. 8 SEM images of TMAZ-HZ showing banding structure (noted only on advancing side of weldment): (a) X80, (b) L80-1

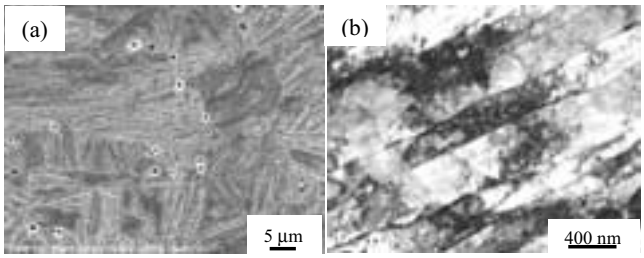

Fig. 9 X80 sample; microstructure of TMAZ-HZ: (a) SEM, (b) TEM showing martensite

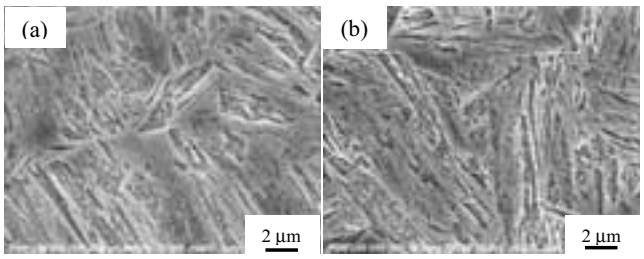

Fig. 10 Microstructure of TMAZ-HZ: (a) L80-1 and (b) L80-2 (SEM images showing martensite)

also observed in the TMAZ-HZ, as shown in the SEM macrographs (Fig. 8).

Figs. 9 and 10 show the microstructures of the TMAZ-HZ in X80 and L80 steels, respectively. In all the samples investigated, the TMAZ-HZ was composed predominantly of acicular microstructure, a mixture of LM, DUB and LB, consistent with its high hardness.

Another microstructural feature noted in the TMAZ-HZ is the presence of second-phase inclusions (Fig. 11). One set of particles was coarse (2∼5 μm) and spherical in shape; these were identified as aluminum oxide. A second set of particles was angular in morphology and ranged in size from 0.2 to 5 μm. SEM EDS from the second set of particles show B, N peaks as major constituents, indicating these particles may be debris from the PCBN tool.

SIMS analysis has also been performed in the TMAZ-HZ and TMAZ regions of the X80 sample to compare the boron content in these regions. Figs. 12a and b are SIMS images of boron in the TMAZ HZ and TMAZ of X80, respectively. SIMS results reveal that B-containing particles are confined to the TMAZ-HZ; this observation also suggests that some boron may have been dissolved in solid solution in the TMAZ-HZ.

DISCUSSION

The results of this study indicate that both X-80 and L-80 can be welded by FSW. In order to evaluate the relative merits of

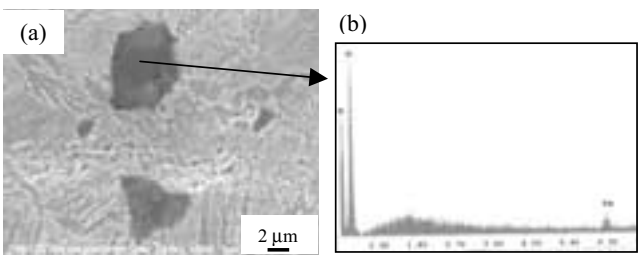

Fig. 11 Inclusions in TMAZ-HZ: (a) SEM image showing angular inclusions and (b) EDS spectrum from inclusions

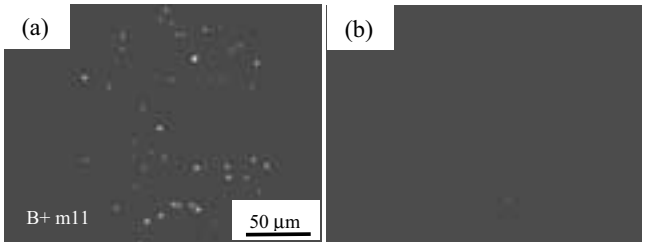

Fig. 12 SIMS images of boron from X80 FSW: (a) TMAZ-HZ and (b) TMAZ

FSW compared to fusion welding (FW), it is first necessary to compare the microstructures of FSW with those achieved in conventional FW. However, a quantitative comparison between the 2 joining methods is possible only when the key process parameter, viz. heat input, is kept constant for the 2 methods. Because this was not the case in this study, only a qualitative comparison is presented here for the X80 and L80 steels.

X80 Steel

1. In the coarse grain region of the HAZ (one of the weakest links in FW) the grain size in FSW is comparable to that of the base metal, of the order of 5 microns. The conventional coarse grain in the HAZ of FW is thus absent in FSW.
2. The grain size in FSW increased from a value of 5 microns in the HAZ to a maximum value of 30 microns in the advancing side of the TMAZ, indicating a coarse grain structure is in the TMAZ and not in the HAZ. The observation implies that the conventional coarse grain structure that forms at the fusion line of FW has been moved to the advancing side of the TMAZ in FSW. However, it should be pointed out that the coarse grains in the TMAZ do not form along a continuous boundary (such as the fusion line) and thus may be less detrimental than the conventional coarse grains in FW.
3. The extent of HAZ softening is considerably less for FSW compared to FW (Fig. 13). The lower HAZ softening is the result of the lower peak temperatures attained in the FSW HAZ. The lower softening is an important feature in preventing fusion line failures in weldments (Koo et al., 2003).
4. The formation of a hard zone in the advancing side of the TMAZ, (TMAZ-HZ) is specific to FSW of the steels investigated. TEM, SEM and SIMS studies suggest that the higher hardness is due to the increased hardenability in this region resulting in the formation of a mixture of high-hardness acicular phases such as LM, DUB and LB. This increased hardenability could result from grain coarsening and boron alloying from the dissolution of BN particles from the tool. Studies are in progress to characterize the solid solution boron in this region.

The comparison presented above shows that, in the welding of X80 steels, FSW offers several key advantages compared to conventional FW. The elimination of contiguous coarse grains at the fusion line and minimization of fusion line softening are extremely attractive attributes of FSW. However, attention may be required to improve the weld metal properties because in the as-welded condition FSW suffers from regions of coarser grains and possibly a local region of higher hardness.

L80 Steel

The regions of interest in the L80 weldment are different in X80 steels. For instance, softening at the fusion line is not relevant as a result of the higher hardenability of the steel. Instead,

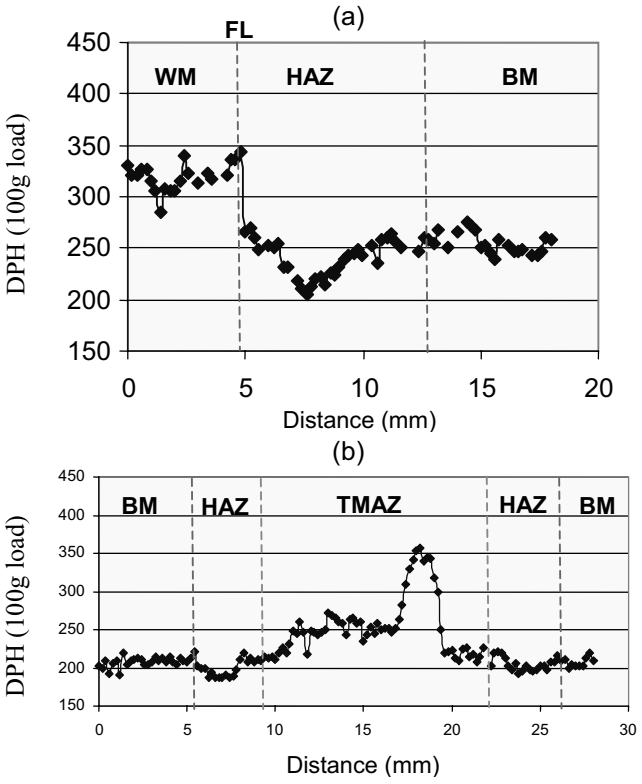

Fig. 13 Microhardness profiles of X80 steel: (a) FW, (b) FSW

formation of high hardness regions in the HAZ due to improper post-weld heat treatment would be of concern. Fig. 2 shows the hardness profiles of the welds of the L80 steel prepared by 2 process conditions. The results indicate that the weld hardness can be altered by the process parameters. Decreasing the RPM of the tool by 100 resulted in the drop of weld hardness by about 75 DPH. This result indicates that there is considerable room to control the weld hardness by appropriate control of FSW parameters.

CONCLUSIONS

The results of this preliminary study show that FSW has the potential to successfully join steels with different carbon contents and processing histories. Both steels were welded without any macroscopic defects.

In the thermomechanically processed X80 steel, the FSW joint resulted in relatively fine grains (5 to 7 μm) in the HAZ with minimal softening. The grains in the hard zone of the TMAZ were coarser, of the order of 30 μm. The combination of grain size, strain and temperature in the HAZ and TMAZ resulted in a range of microstructures consisting of a combination of granular bainite and lath martensite.

In the quenched and tempered L80 steel, the microstructure of the FSW weldment consisted of lower bainite, degenerate upper bainite and tempered martensite. The hardnesses of the welded regions were dependent on the FSW tool rotation speed and were higher than that of the base metals. The results suggest that the hardness of the weldment can be tailored by controlling the FSW parameters (e.g. rotation speed, travel speed and Z-load).

Future efforts in FSW of carbon steels should concentrate on optimizing the microstructure and properties of the weldment, particularly the TMAZ, which is exposed to the highest temperatures in the process.

REFERENCES

Bangaru, NV, Fairchid, DP, Macia, ML, Koo, JY, and Ozekcin, A (2004). "Microstructural Aspects of High Strength Pipeline Girth Welds," *Pipeline Tech 2004*, Ostend, Belgium, pp 789.

Johnson, R, Dos Santos, J, and Magnasco, M (2003). "Mechanical Properties of Friction Stir Welded S355 C-Mn Steel Plates," *4th Int Friction Stir Welding Symp*, Park City, Utah, USA, in CD-ROM (not paginated).

Honeycombe, RWK, and Bhadeshia, HKDH (1995). *Steels: Microstructure and Properties*, Edward Arnold, Division of Hodder Headline PLC.

Konkol, P (2003). "Characterization of Friction Stir Weldments in 500 Brinell Hardness Quenched and Tempered Steel," *4th Int Friction Stir Welding Symp*, Park City, Utah, USA, in CD-ROM (not paginated).

Koo, JY, Luton, MJ, Bangaru, NV, Petkovic, RA, Fairchild, DP, Petersen, CW, Asahi, H, Hara, T, Terada, Y, Sugiyama, M, Tamehiro, H, Komizo, Y, Okaguchi, S, Hamada, M, Yamamoto, A, and Takeuchi, I (2003). "Metallurgical Design of Ultra-high Strength Steels for Gas Pipelines," *Proc 13th Int Offshore and Polar Eng Conf,* Honolulu, ISOPE, Vol 4, pp. 10–18.

Lienert, TJ, Stellwag, WL, Grimmett, BB, and Warke, RW (2003). "Friction Stir Welding Studies on Mild Steel," *Welding Res, Supplt to Welding J*, AWS p 1-S.

Lienert, TJ, Tang, W, and Kvidahl, LG (2003). "Friction Stir Welding of DH-36 Steel," *4th Int Friction Stir Welding Symp*, Park City, Utah, USA, in CD-ROM (not paginated).

Okamoto, K, Hirano, S, Inagaki, M, Park, SHC, Sato, YS, Kokawa, H, Nelson, T, and Sorensen, CD (2003). "Metallurgical and Mechanical Properties of Friction Stir Welded Stainless Steels," *4th Int Friction Stir Welding Symp*, Park City, Utah, USA, in CD-ROM (not paginated).

Packer, S, Nelson, T, Sorensen, CD, Steel, R, and Matsunaga, M (2003). "Tool and Equip Requirements for Friction Stir Welding Ferrous and Other High Melting Temperature Alloys," *4th Int Friction Stir Welding Symp*, Park City, Utah, USA, in CD-ROM (not paginated).

Posada, M, DeLoach, J, Reynolds, AP, Fonda, R, and Halpin, J (2003). "Evaluation of Friction Stir Welding HSLA-65," *4th Int Friction Stir Welding Symp*, Park City, Utah, USA, in CD-ROM (not paginated).

Reynolds, AP, et al. (2003). "Structure, Properties, and Residual Stress of 304L Stainless Steel Friction Stir Weld," Scripta Mater, Vol 48, p 1289.

Threadgill, P, and Johnson, R (2004). "The Potential for Friction Stir Welding in Oil and Gas Application," *Proc 14th Int Offshore and Polar Eng Conf,* Toulon, France, ISOPE, pp. 1–7.

Threadgill, PL, and Leonard, AJ (1999). "Macro and Microstructural Features of Friction Stir Welds in Various Materials," TWI Rept.

Thomas, MW, Nicholas, ED, Needham, JC, Murch, MG, Templesmith, P, and Dawes, CJ (1991). GB patent application No. 9125978.8.